

Extracting changes in air temperature using acoustic coda phase delays

Omar Marcillo,^{a)} Stephen Arrowsmith, Rod Whitaker, Emily Morton,
and W. Scott Phillips

*Geophysics Group, Los Alamos National Laboratory, P. O. Box 1663, Los Alamos,
New Mexico 87545*

omarcillo@lanl.gov, arrows@lanl.gov, rww@lanl.gov, emorton@lanl.gov, wsp@lanl.gov

Abstract: Blast waves produced by 60 high-explosive detonations were recorded at short distances (few hundreds of meters); the corresponding waveforms show charge-configuration independent coda-like features (i.e., similar shapes, amplitudes, and phases) lasting several seconds. These features are modeled as reflected and/or scattered waves by acoustic reflectors/scatters surrounding the explosions. Using explosion pairs, relative coda phase delays are extracted and modeled as changes in sound speed due to changes in air temperature. Measurements from nearby weather towers are used for validation.

PACS numbers: 43.28.Vd, 43.28.We, 43.28.Mw, 43.28.Bj [VO]

Date Received: May 6, 2014 **Date Accepted:** September 14, 2014

1. Introduction

Blast waves are defined as an abrupt jump in pressure followed by an immediate decay after a peak is reached (density and acoustic particle velocity follow the same pattern). The detonation of high explosives (HE) or mixtures of volatile gases can generate blast waves (Needham, 2010). The duration of the overpressure above and below ambient pressure, for the first time after the arrival of the shock, are called positive and negative phases, respectively. The amplitude of the waveform after these two main components is highly attenuated and reaches ambient noise levels in few seconds. We found, by studying a series of small HE detonations (between 1 and 15 kg) recorded at less than 1 km with the same source-receiver geometry, that the signal after the negative phase has features that repeat in amplitude and phase consistently between explosions. We call this part of the signal the acoustic coda.

Seismic coda waves have been defined as a signal (different from background noise) present in a seismogram after the arrival of major wave types, i.e., P, S, and surface waves, and are commonly interpreted as the result of backscattering by heterogeneities in the propagation media (Aki and Chouet, 1975). Seismic codas are considered the thumbprint of the media's heterogeneities and thus have been extensively studied (see Herraiz and Espinosa, 1987). For example, small phase shifts in codas have been used to monitor small changes in the medium configuration (Snieder, 2006). Poupinet *et al.* (1984) modeled small phase delays as changes in crustal velocities, Roberts *et al.* (1992) modeled similar behavior in laboratory samples and included estimates of attenuation (quantified in the seismic community by the parameter Q), and Ratdompurbo and Poupinet (1995) used the same approach and suggested a change in velocity related to changes in the pressure in a volcanic chamber. For acoustic signals propagating in the atmosphere, Perepelkin *et al.* (2011) and Blom and Waxler (2012) identified specific elements in acoustic codas to characterize various aspects of the vertical sound speed profiles in the nocturnal boundary layer. We show in this work a technique to extract relative changes in air temperature; the technique is based

^{a)} Author to whom correspondence should be addressed.

on comparing the codas from explosion pairs, measuring relative phase delays, and extracting air temperature ratios.

2. Instrumentation and data

A group of HE detonations (Composition B) were conducted at Los Alamos National Laboratory; the explosions comprised charges with different shapes (cylinders and spheres), height of bursts (HOBs; -1, 0, 0.5, 1, 2, and 4 m), and masses (1, 4, 11, 14 kg). Exploding bridgewire detonators fired the charges. A rope traversing two concrete-block towers was used to suspend the charges. This allowed us to fire the charges at varying heights with minimal interference from experimental infrastructure. The instrumentation for this experiment comprised: (1) four stations (TRE, RDG, MOM, MOH) with InfraNMT sensors (Marcillo *et al.*, 2012) located at different distances (0.23, 0.29, 0.8, and 0.81 km) and azimuths (77°, -94°, 77°, and 71°) from the shot pit [Fig. 1(a)], and (2) data from two weather towers (TA-6 and TA-54, not shown in the map) located (relative to the shot pit) at 5.3 and 5 km with azimuths of 315° and 91°, respectively. The recording systems were set to sample and store 1000 samples per second. Figures 1(b) and 1(c) show the waveforms from explosions #93 (sphere, 14.9 kg) and #99 (cylinder, 11.6 kg) recorded at the closest sensor (TRE). Both explosions had a HOB of 4 m. These waveforms display similar shapes for the positive phases; higher maximum amplitudes correspond to heavier charges as expected. The negative phases, however, are different; the cylindrical charge shows a local maximum between 40–50 ms not seen in waveforms from spherical charges. This peak is present in most of the cylindrical charges and can be related to a more complex radiation pattern (Knock and Davies, 2013) and its interaction with the surroundings. The negative phases are followed by very rapid amplitude attenuation. Figure 1(d) shows both waveforms side by side in a larger time window (5 s after the onset of the signals) and shorter pressure scale (± 10 Pa). Note the similarity between the signals in shape,

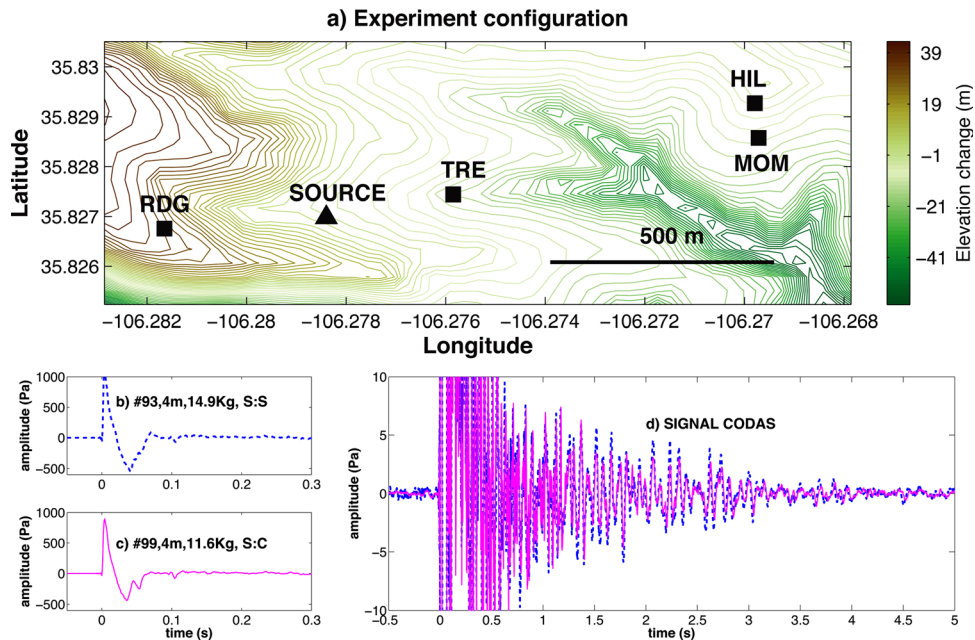


FIG. 1. (Color online) Sensor distribution and examples of recorded signals. (a) The location of the sensor stations (squares) and shot pit (triangle). (b) and (c) The initial 0.3 s of explosions #93 (dashed line) and #99 (solid line) recorded by station TRE. (d) The initial 5 s for the explosions of (b) and (c) with the signals side by side for comparison.

relative location, and amplitude, and the slight phase delay that appears to increase with time.

2.1 Cross-correlograms

We use a cross-correlogram (XC) technique to measure the degree of similarity between the different sections of the signals; we are following the approach described by Poupinet *et al.* (1984) but are comparing the signals in the time domain. To construct our XCs, we compute the cross-correlation between corresponding sliding windows in the waveforms. The coefficients of the cross-correlation for each window are color-coded and mapped on a 2D plot. We perform the cross-correlation using 0.2-s moving windows with 0.15-s overlap. Figures 2(a) and 2(b) show the signals and XCs corresponding to the explosions described in Figs. 1(b) and 1(c) recorded by stations TRE and RDG, respectively. Figures 2(c) and 2(d) show the signals and the corresponding XCs for explosions #49 and #99 recorded at TRE and RDG stations, respectively. Explosion #49 corresponds to a 4.9 kg charge with cylindrical shape and a HOB of 4 m.

The XCs display three main features: (1) localized times with high cross-correlation, (2) a slope in the sections with high correlation coefficients (main trend), and (3) short time windows with different slopes embedded in the main trend. The sections with high correlation coefficients in the XCs (feature 1) have similar shapes and relative locations for different explosion pairs recorded by the same station, for example, compare Figs. 2(a) and 2(c). The shape and relative location of these sections are different for the same explosion pair recorded at different stations. Feature 2, the slope in the sections with high correlation coefficients, has similar values in XCs of the same explosion pair at different stations, for example, compare Figs. 2(a) and 2(b); the slope

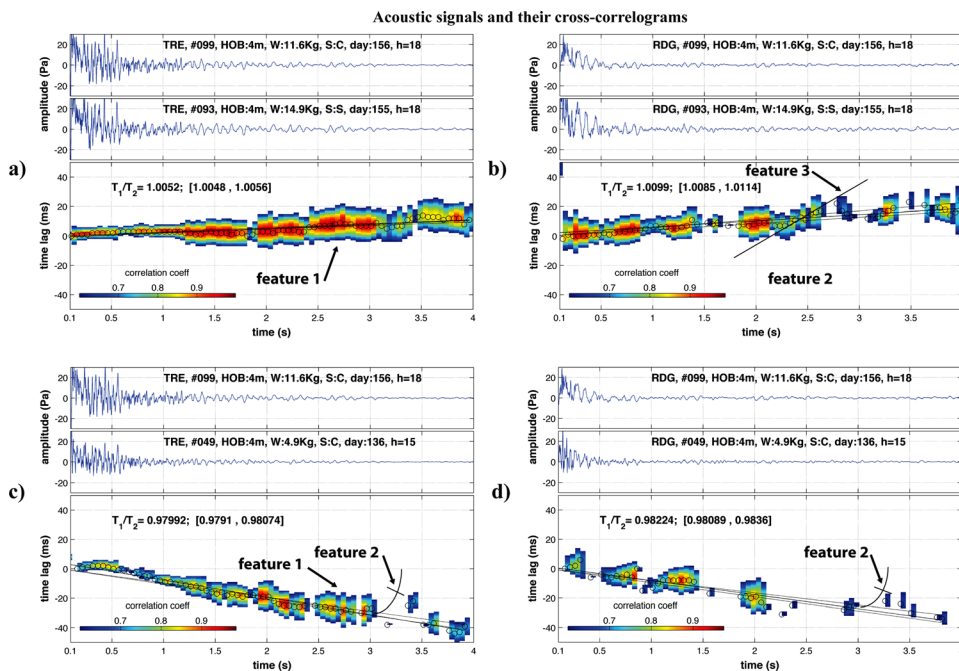


FIG. 2. (Color online) Examples of the acoustic signals and their cross-correlograms. (a) and (c) The explosion signals and the XCs between explosions #93 and #49 using explosion # 99 as reference for station TRE; (b) and (d) The corresponding signals and XCs for station RDG. The cross-correlograms use a sliding window of 0.2 s and 0.15 s overlapping. Temperature ratios extracted from the coda analysis with corresponding 95% confidence intervals (inside the square brackets) are also shown.

is different for different explosion pairs. Feature 3 is variable between different explosion pairs and different stations.

We modeled the features found in the XCs using the presence of scattering elements (feature 1), changes in air temperature (feature 2), and wind (feature 3). Infrastructure (e.g., concrete towers) and other physical objects around the explosions (e.g., ground, trees) can scatter and/or reflect the incoming blast wave; as the source-receiver geometry and topography does not change, feature 1 is persistent between the explosions and specific for each station. Changes in air temperature affect the sound speed and the relative location of the scattered/reflected waves in the coda; thus, the coda is stretched and compressed with lower and higher temperatures, respectively. Feature 2 is the result of the changes in air temperature between explosions. As temperature affects the sound speed isotropically, so we see similar slopes at different stations for the same pair of explosions [Figs. 2(a) and 2(b)]. On the other hand, wind is a vector and its influence on sound speed depends on the projection of the wind in the direction of propagation. We speculate that feature 3 depends strongly on the wind and source-scatter-receiver geometry. As the detonations were conducted in a facility that requires low-wind conditions for testing, feature 3 is not a strong element in the recorded codas.

3. Air temperature and its influence on the coda phases

The velocity of sound in the air is controlled by the air temperature (T), wind (\mathbf{w} , the vector wind velocity), and the direction of propagation (\mathbf{n} , the dimensionless unit vector normal to the wavefront). We define effective sound speed (c_{eff}) as a magnitude to account for these parameters as $c_{eff} = c + \mathbf{n} \cdot \mathbf{w}$, where $c = c(T) \cong 20.06\sqrt{T}$ corresponds to the adiabatic sound speed, T is the absolute temperature (K), and the term $\mathbf{n} \cdot \mathbf{w}$ corresponds to the dot product between the propagation and wind vectors. This equation shows that changes in air temperature have an isotropic effect in the sound speed, while changes in the wind vector have an anisotropic effect as it depends of the projection of the wind along the vector normal to the wavefront.

We have defined the coda as the result of waves scattered by high impedance elements in the environment and subsequently recorded at the receiver after the first arrival. We now define $\Delta d^i = d^{\beta i} + d^{i\chi} - d^{\beta\chi}$, where d^{ab} corresponds to the radial distance between a and b , the superscripts β , i , and χ correspond to source, i th scatter/reflector, and receiver, respectively. Assuming that two explosions (identified by subscripts 1 and 2) have the same source and receiver locations and scattering elements, we can write $\Delta d_1^i = \Delta d_2^i$, where the subscript identifies the explosions; we can also write $\Delta d_1^i = c_1(T_1)t_1^i$, where t_1^i corresponds to the arrival time of the signal scattered by the i th element relative to the direct arrival. As the air temperature can change between explosions, we write

$$c_1(T_1)t_1^i = c_2(T_2)t_2^i. \tag{1}$$

Using XCs, we can extract phase delays in the codas of a pair of explosions and write $t_2^i = (t_1^i + \delta t^i)$. Using the dependence of the air temperature and adiabatic sound speed, we can write Eq. (1) as

$$\frac{T_1}{T_2} = \left(1 + \frac{\delta t^i}{t_1^i}\right)^2. \tag{2}$$

Using the maximum cross-correlation value in the XCs, we can extract points for each sliding window and fit a linear equation to the set of points. Equation (2) can now be used to derive temperature ratios using the slope of the fitted curve. Figure 3(a) shows the estimated temperature ratios obtained by applying the coda analysis to all the explosions of the dataset for station TRE. We see the same behavior for the temperature ratios extracted using the signals from the other stations. As TRE is the

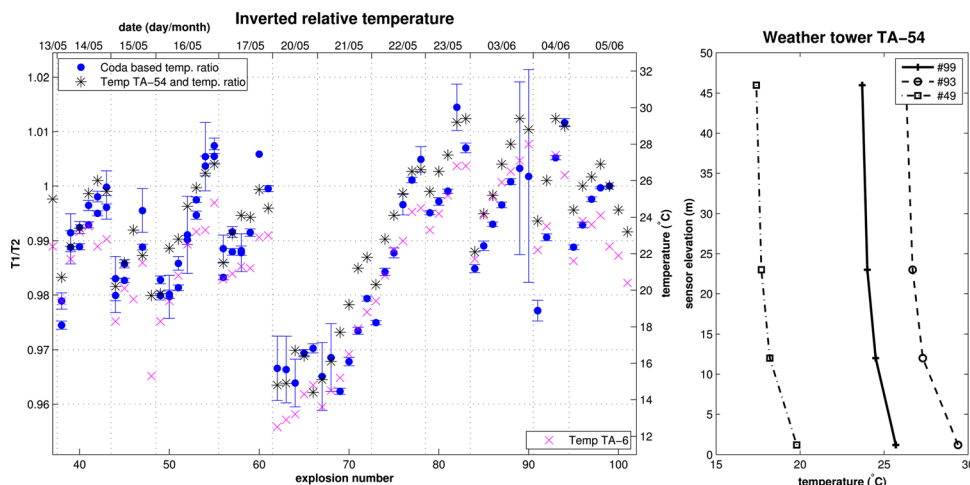


FIG. 3. (Color online) (a) Air temperature ratios from nearby weather towers (asterisks and crosses) and temperature ratios (dots) extracted using coda analysis (and corresponding 95% confidence intervals, error bars), explosion #99 is used as reference. (b) Air temperature profiles from nearby weather tower for the explosions in Fig. 2. The large confidence intervals for the ratios for explosions #89 and #90 can be related to a more distributed source as these charges were buried 1 m below ground.

closest station and the one with higher signal-to-noise ratios, the inverted temperature ratios are better constrained (smaller confidence intervals). We are using explosion #99 as a reference for all the XCs. We use air temperature recorded by nearby weather towers to validate our approach. Figure 3(b) shows the vertical temperature for a subset of explosions. As the profiles show a negative gradient, we expect the acoustic energy to reach the sensors by traveling mainly horizontally, without significant refraction.

4. Discussion

Figure 3 shows that the coda-based ratios follow the air temperature measurements from nearby weather towers. The temperature measurements from both towers show differences up to 3 °C between each other, with TA-54 having consistently higher values than TA-6; these differences can be related to local effects such as vegetation, cloud coverage, or topography. Our inversion follows the main feature (note ratios between explosions 60 and 80, between 20/5 and 23/5, Fig. 3) and most of the small features (between explosions 78 and 82) in air temperature with values consistently between the temperatures from the weather towers. As the waves in the coda travel different distances in all directions around the source before reaching the sensor, local changes in air temperature are averaged. Thus, the technique described here provides a bulk estimation of the relative air temperature that we suggest is less sensitive to local effects. Also, as this technique uses only relative changes in the coda, precise ground-truth information is not required.

Our technique relies on distinguishing the coda from the background noise. This requirement is easily met for blast waves recorded at short distances under low wind conditions. For other scenarios where this technique could be applied, such as volcanic explosions or lightning, the signal-to-noise ratio for the coda can be lower. For those cases, very small aperture arrays could be used to enhance the coda; these arrays could also provide information of the relative location of the scattering elements. As the changes in phase can be on the order of milliseconds, a sampling rate in excess of 1 kHz could increase the applicability of our technique.

Feature 3, present in some of the XCs, is suggested as the result of wind in one or both of the explosion pairs. Different from the influence of temperature, wind

affects the propagation preferentially. Modeling the influence of the wind would require knowing the specific location of scattering points and using a reference explosion without wind. This may introduce more constraints but has the potential of extending our technique to recover wind and temperature simultaneously.

5. Conclusions

By analyzing blast waves from chemical explosion, we found features that repeat in amplitude and phase consistently between explosions and can last several seconds; we call this part of the signal the acoustic coda. By using the acoustic coda, we have demonstrated a technique to recover differential air temperatures around explosions. This technique provides an estimation of changes in bulk air temperature that has less sensitivity to very local atmospheric changes. Also, as the coda is very sensitive to changes in the location of background scatters, this technique can provide information on changes in source location between explosions. Some volcanoes can provide favorable conditions to apply our technique (for example, see [Marchetti *et al.*, 2013](#)); i.e., loud and highly repetitive sources and very distinctive topography (e.g., crater walls and domes). For these environments, our technique could provide information of changes in temperature and wind that could be used to complement other direct atmospheric measurements.

Acknowledgments

This work was funded by the Office of Defense Nuclear Nonproliferation Research and Development within the U.S. Department of Energy's National Nuclear Security Administration. This work was performed under the auspices of the U.S. Department of Energy by Los Alamos National Laboratory under Contract DE-AC52-06NA25396.

References and links

- Aki, K., and Chouet, B. (1975). "Origin of coda waves: Source, attenuation, and scattering effects," *J. Geophys. Res.* **80**(23), 3322–3342, doi:10.1029/JB080i023p03322.
- Blom, P., and Waxler, R. (2012). "Impulse propagation in the nocturnal boundary layer: Analysis of the geometric component," *J. Acoust. Soc. Am.* **131**(5), 3680–3690.
- Herraiz, M., and Espinosa, A. F. (1987). "Coda waves: A review," *Pure Appl. Geophys.* **125**(4), 499–577.
- Knock, C., and Davies, N. (2013). "Blast waves from cylindrical charges," *Shock Waves* **23**(4), 337–343.
- Marchetti, E., Ripepe, M., Delle Donne, D., Genco, R., Finizola, A., and Garaebiti, E. (2013). "Blast waves from violent explosive activity at Yasur Volcano, Vanuatu," *Geophys. Res. Lett.* **40**(22), 5838–5843, doi:10.1002/2013GL057900.
- Marcillo, O., Johnson, J. B., and Hart, D. (2012). "Implementation, characterization, and evaluation of an inexpensive low-power low-noise infrasound sensor based on a micromachined differential pressure transducer and a mechanical filter," *J. Atmos. Oceanic Technol.* **29**(9), 1275–1284.
- Needham, C. (2010). *Blast Wave Propagation. Blast Waves* (Springer, Berlin), 336 pp.
- Perepelkin, V. G., Kulichkov, S. N., Chunchuzov, I. P., and Kuznetsov, R. D. (2011). "On Experience in using the remote acoustic method of partial reflections in studies of the lower troposphere, *Izvestiya*," *Atmos. Oceanic Phys.* **47**(1), 1–14.
- Poupinet, G., Ellsworth, W. L., and Frechet, J. (1984). "Monitoring velocity variations in the crust using earthquake doublets: An application to the Calaveras Fault, California," *J. Geophys. Res.* **89**(B7), 5719–5731, doi:10.1029/JB089iB07p05719.
- Ratomopurbo, A., and Poupinet, G. (1995). "Monitoring a temporal change of seismic velocity in a volcano: Application to the 1992 eruption of Mt. Merapi (Indonesia)," *Geophys. Res. Lett.* **22**(7), 775–778, doi:10.1029/95GL00302.
- Roberts, P. M., Phillips, W. S., and Fehler, M. C. (1992). "Development of the active doublet method for measuring small velocity and attenuation changes in solids," *J. Acoust. Soc. Am.* **91**(6), 3291–3302.
- Snieder, R. (2006). "The theory of coda wave interferometry," *Pure Appl. Geophys.* **163**(2–3), 455–473.